

Original Article

## Formation process of cover collapse sinkholes related to groundwater level decline in karst areas

**LIU Xingzong**<sup>1</sup>  <https://orcid.org/0000-0003-4383-3777>; e-mail: liu\_xingzong@163.com

**CHEN Hongkai**<sup>2</sup>  <https://orcid.org/0000-0001-6477-7108>; e-mail: chk658@163.com

**GONG Bin**<sup>3\*</sup>  <https://orcid.org/0000-0002-9464-3423>;  e-mail: bin.gong@brunel.ac.uk

**JIANG Guanghui**<sup>1</sup>  <https://orcid.org/0000-0003-3142-8803>; e-mail: jgh@ldu.edu.cn

**WANG Jintao**<sup>1</sup>  <https://orcid.org/0000-0001-7557-2490>; e-mail: wangjintao@ldu.edu.cn

\*Corresponding author

<sup>1</sup> School of Civil Engineering, Ludong University, Yantai 264025, China

<sup>2</sup> School of Geographical Sciences, China West Normal University, Nanchong 637001, China

<sup>3</sup> College of Engineering, Design and Physical Sciences, Brunel University London, London UB8 3PH, UK

**Citation:** Liu XZ, Chen HK, Gong B, et al. (2024) Formation process of cover collapse sinkholes related to groundwater level decline in karst areas. Journal of Mountain Science 21(11). <https://doi.org/10.1007/s11629-024-8944-x>

© The Author(s) 2024.

**Abstract:** The decline in groundwater level is a key factor contributing to cover collapse in karst areas. In this study, the model tests and numerical simulations are conducted to reveal the breeding process and formation mechanism of cover collapse sinkholes caused by the decline of groundwater level in karst area. Firstly, the model tests confirm that the decline of groundwater level generates negative pressure at the lower edge of overlying soil. The negative pressure experiences four distinct phases during the groundwater drawdown process: rapid rise, slow decline, rapid decline, and gradual dissipation. The maximum negative pressure is influenced by the particle size distribution of the overlying soil. Then, the numerical simulations are carried out to investigate the change process of negative pressure caused by the loss of fillers in karst pipe. The simulated results indicate that the rate of groundwater decline and the thickness and initial void ratio of the overlying soil can affect the maximum negative pressure. As groundwater level drops, a negative pressure zone forms underground, causing tensile failure in the

surrounding soil and creating an arched soil hole, which weakens the support for the overlying soil. This phenomenon can also lead to the collapse of the overlying soil under its self-weight. Groundwater table decline in karst areas can result in both internal and surface collapses. When the overlying soil is thin, internal and surface collapses occur simultaneously. In contrast, for thick overlying soil, internal collapse happens first, followed by a layer-by-layer collapse, ultimately forming sinkholes. Finally, the breeding process and formation mechanism of the Yujiawan Reservoir sinkholes are discussed. Geological conditions and groundwater level decline significantly affect internal collapse in karst areas, requiring careful consideration from on-site engineers.

**Keywords:** Cover collapse sinkhole; Groundwater level decline; Karst area; Model test; Numerical simulation

### 1 Introduction

Cover collapse sinkhole in karst areas is a kind of

**Received:** 01-Jun-2024  
**Revised:** 27-Aug-2024  
**Accepted:** 21-Sep-2024

complicated environmental and geological hazards (Gutierrez et al. 2014). This type of hazards has been reported in many countries around the world (Gutierrez et al. 2008; Margiotta et al. 2016; Luu et al. 2019; Malinowska et al. 2019; Dong et al. 2020; Lago et al. 2022; Talib et al. 2022; Brahmi et al. 2023). The cover collapse sinkholes can occur in both urban and rural areas, endangering not only people's lives but also roads, farmlands, and other facilities (Dai and Lei 2018; di Santolo et al. 2018; Liu et al. 2023; Zhang et al. 2023). The influencing factors of the collapse of underground voids can be divided into natural factors and anthropogenic factors. The natural factors include geological conditions (Chen et al. 2022), geomaterial parameters (Feng et al. 2024; Gao et al. 2023; Liu et al. 2024), rainfall (Qin et al. 2023), earthquakes (Pei et al. 2023) and so on, while the anthropogenic factors include over-pumping of groundwater (He et al. 2013; Howari et al. 2016; Meng et al. 2020), roadway construction (Zhou and Beck 2005), mining (Kharisova et al. 2021; Yao et al. 2022), and other underground engineering excavations (Zhang et al. 2022; Seol et al. 2022; Xu et al. 2024). Cover collapse sinkholes caused by human activities are usually large-scale and sudden (He et al. 2002; Festa et al. 2012). Numerous studies show that groundwater level decline caused by human activities is a key factor resulting in the cover collapse sinkholes in karst areas (He et al. 2010; Zhao et al. 2012; He et al. 2012; Xia et al. 2019; Zeng and Zhou 2019). So far, the formation of cover collapse sinkholes caused by the decline in groundwater level can be explained by the potential erosion theory (White 2002; Pan et al. 2022) and the vacuum absorption erosion theory (Jiang et al. 2018; Pan et al. 2018). The potential erosion theory states that soil particles are carried away by water over time, and a cave gradually forms. While the vacuum absorption erosion theory emphasizes that a cave with low air pressure forms after water table drops. The low air pressure cave has two adverse effects: the stretching of the floor of soil and the atmospheric pressure of the top of soil. These two adverse effects make the ground prone to collapse.

The reduced air pressure caused by the groundwater level decline creates tensile stresses on the bedrock surface, which may lead to the sinkhole formation. In view of this situation, many scientists use mechanical models to study cover collapse sinkholes (Galve et al. 2011; Wei and Sun 2018; Jia et al. 2018). With the development of numerical calculation

technology, the methods of finite element method (Gong et al. 2022; Yu et al. 2022; Wang et al. 2023; Yu et al. 2024), finite difference method (Yacine et al. 2014), discrete element method (Al-Halbouni et al. 2019; Zhang et al. 2024; Zhu 2024) and coupled continuum-discontinuum methods (Gong et al. 2024; Wang et al. 2024) are used to study the failure of geological structures, e.g., the cover collapse sinkholes caused by groundwater decline. In addition to theoretical analysis and numerical calculation methods, field monitoring (Jiang et al. 2017; Jiang et al. 2019; Jia et al. 2021), in-situ tests (Zumpano et al. 2019; Liang et al. 2020) and laboratory model tests (Guo et al. 2014; Xiao et al. 2018; Guo et al. 2023; Peng et al. 2023) are also commonly used research methods to determine the mechanism and main influencing factors of cover collapse sinkholes caused by groundwater level decline.

The previous studies mainly aim to reveal the inducing factors of cover collapse sinkholes, such as water erosion and changes in air pressure, and pay little attention to the formation process and influencing factors of cover collapse sinkholes (Jiang et al. 2018; Pan et al. 2018; Pan et al. 2022). However, the cover collapse sinkholes caused by groundwater level decline do not always happen suddenly. For example, from October 20, 2010 to September 13, 2015, six sinkholes occurred successively at the east of the Yujiawan Reservoir in China. Therefore, the progressive formation process and breeding conditions of cover collapse sinkholes caused by groundwater level decline in karst areas still need to be comprehensively investigated. In this study, the presence of negative pressure after groundwater decline was confirmed using the model experiments. Then, the numerical simulations were performed to clarify the variation law of negative pressure as the groundwater level decreased and to analyze the influencing factors of negative pressure. Based on the results of model tests and numerical simulations, the formation process of cover collapse sinkholes in karst areas was explained. Finally, the breeding process and formation mechanism of the Yujiawan Reservoir sinkholes were revealed by numerical simulation.

## 2 Model Tests of Groundwater Level Decline

As groundwater levels decline, negative pressure zones may form beneath the relatively impermeable overlying soil. However, the overlying soil is in reality not completely impermeable. In the overlying soil that

are not completely sealed, the inner air pressure is basically a balance between pressure replenishment and consumption. The decline in groundwater level leads to a reduction in air pressure beneath the overlying soil, while air pressure is continuously replenished from the pores and fissures of the soil. Therefore, the pores and cracks of the overlying soil may be key factors affecting the magnitude of the negative pressure beneath the overlying soil. In this section, the model tests are used to investigate the negative pressure caused by the decline in groundwater level.

### 2.1 Experimental equipment

In this experiment, a device was developed to simulate ground subsidence caused by the decline in groundwater level. The device mainly consists of an iron experimental chamber and pressure measuring

devices (Fig. 1). The iron experimental chamber has the dimensions of 0.6 m in length, width and height and is divided into two parts by a layer of geotechnical fabric covered iron gauze. The upper part is filled with clay to simulate the overlying soil, while the lower part is filled with water to simulate groundwater. The pressure transmitters have a response pressure of -100 kPa to 100 kPa, which are placed at the bottom of the clay layer and can convert the pressure at the bottom of the clay layer into a digital signal that is transmitted to the computer.

### 2.2 Materials

The large clods in the original clay are broken up, and the crushed stone in the clay is removed by screening to obtain an artificial silty clay without crushed stone (Fig. 2). Four types of gravel with different particle sizes (0.15 mm~5 mm, 5 mm~10 mm,

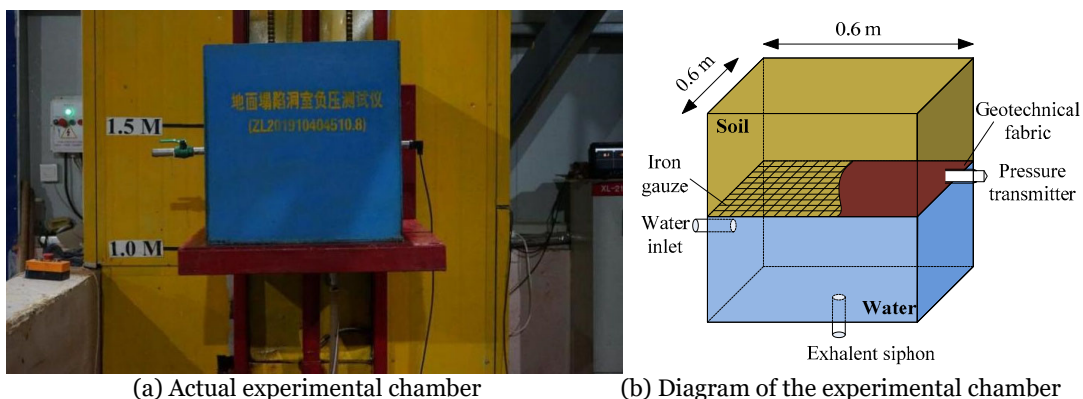


Fig. 1 Schematic illustration of the experimental chamber used for the water-level decline model test.

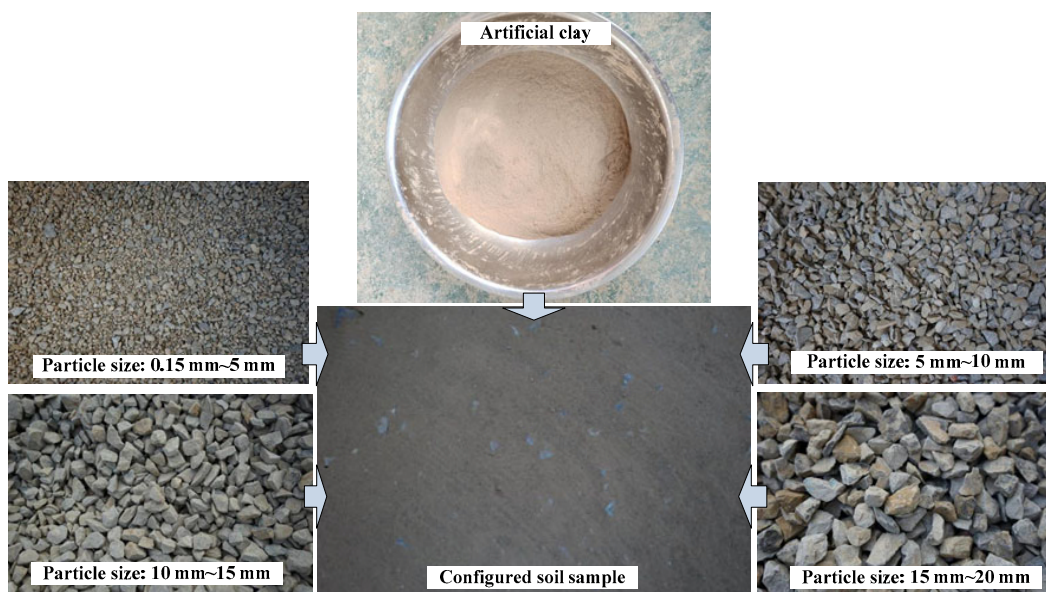


Fig. 2 Materials used for the water-level decline model test.

10 mm~15 mm and 15 mm~20 mm) shown in Fig. 2 are selected and mixed in different ratios to obtain three kinds of gravel samples with different particle size distributions, numbered as JP1, JP2 and JP3, respectively. The particle size distribution curves of the gravel samples are shown in Fig. 3. The gravel samples and artificial clay are mixed to simulate the soil in real-world scenarios. The parameter rock-soil ratio is defined as the ratio of the volume of gravel to the volume of clay in the sample, symbolized by  $R/S$ . In this study, the rock-soil ratios are set to 0.4, 0.2, and 0.1, respectively. The samples are prepared according to the experimental requirements and then poured into the upper part of the iron experimental chamber in batches, stirring during pouring to achieve the most even distribution of the crushed stones in the soil. After compacting the samples, water is added and allowed to sit for 12 hours for natural consolidation and stabilization.

### 2.3 Experimental results

The negative pressure appears at the bottom of the clay layer when water level declines. Under different working conditions, the variation of negative pressure in the sample follows a similar pattern. Taking the condition of using JP3 gravel with the  $R/S$  of 0.1 as an example, the curve of negative pressure variation over time is shown in Fig. 4. The negative pressure in the sample can be divided into four stages over time during the groundwater drawdown process: rapid increase, slow decrease, rapid decrease, and gradual dissipation. At the beginning of the experiment, the air pressure inside the chamber is essentially the same as the atmospheric pressure outside. At this point, the valve at the bottom of the exhalent siphon is opened, allowing water to flow out of the pipe. Due to the sealed nature of the chamber and the saturation of the soil, a negative pressure zone is created at the bottom of the clay. When the water level drops rapidly, the negative pressure quickly increases to its maximum value, which is called the stage of rapid increase of negative pressure. During the increase in negative pressure, tensile cracks develop in the overlying soil layer, allowing external atmosphere to pass through the cracks into the negative pressure zone. Since the formation of cracks in the soil takes a certain time, the negative pressure in the sample slowly decreases and the water linkage from the pipe slows down, which marks the stage of slow decrease of negative pressure.

Due to the development of cracks in the soil, a large amount of air can enter the negative pressure zone through the soil cracks, the negative pressure rapidly releases through the soil cracks, resulting in a rapid decrease of negative pressure. This stage is called rapid decrease of negative pressure. The soil sinks under the action of negative pressure, and when the soil regains stability, the number of cracks in the soil decreases, thereby reducing the penetration of external gas into the soil and gradually releasing the negative pressure in the sample.

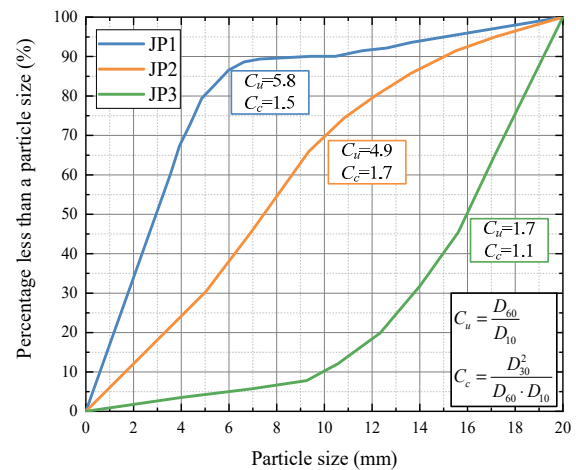


Fig. 3 Particle size distribution curves of the gravel samples.

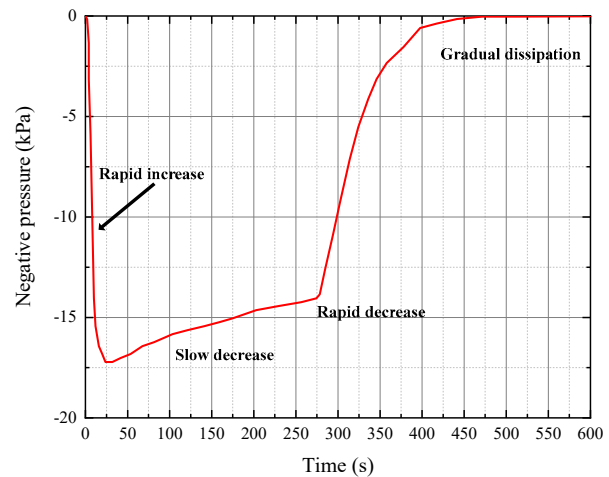


Fig. 4 Negative pressure curve with time (JP3,  $R/S=0.1$ ) ( $R/S$ , the ratio of the volume of gravel to the volume of clay in the sample).

In order to analyze the influencing factors of negative pressure, the maximum negative pressure values obtained under different working conditions are counted in Fig. 5. From the experimental data, it is easy to see that the maximum negative pressure is influenced by the gravel particle size distribution and

the  $R/S$  of the sample. When the  $R/S$  of the sample is relatively high, indicating a higher proportion of gravel in the sample, the influence of the gravel particle size distribution on the negative pressure is not significant. However, if the sample contains a lower proportion of gravel and the added gravel particles are larger, it will result in a noticeable decrease in negative pressure. This is because coarse gravel with a lower proportion in the sample causes the gravel to become isolated and suspended in the clay particles, allowing it to move more easily as the clay particles move, thereby creating larger voids in the sample. This facilitates the entry of outside air into the soil and does not favor the accumulation of negative pressure, resulting in a smaller maximum negative pressure value. For soil samples with a large uniformity coefficient ( $C_u$ ), fine particles are more likely to fill the skeleton formed by coarse particles, so the void ratio of the soil is relatively small (Maroof et al. 2022). Fig. 5 shows that when the gravel proportion is low, the maximum negative pressure decreases as the uniformity coefficient increases. However, when the proportion of gravel is large, the maximum negative pressure increases as the uniformity coefficient increases. Therefore, the maximum negative pressure is affected by the void ratio of the soil and the specific law needs to be further investigated.

### 3 Filler Loss Caused by Groundwater Level Decline

Vertical solution pipes filled with materials are common in karst areas. The decline of groundwater can lead to the loss of fillers in practical engineering. In order to study the change process of negative pressure caused by the decline of groundwater level in practical engineering and its influencing factors, this section uses the numerical technology to simulate the loss process of karst pipe fillers.

#### 3.1 Numerical model

The three-dimensional Fast Lagrange Analysis of Continua (FLAC3D) is used to establish the numerical models. The karst pipe with the diameter of 2 m is set in the limestone rock mass with the dimensions of 14 m in length, 14 m in width and 10 m in height. The pipe is covered by the 2 m thick clay. The middle cross section is displayed to illustrate the model structure in

Fig. 6. The overlying soil layer is calculated as an elastoplastic material, while the limestone and fillers are treated as elastic materials. The loss of karst pipeline fillers caused by the decline of groundwater level in practical engineering leads to the disturbance of overlying soil. Therefore, a vertical downward displacement of  $5 \times 10^{-3}$  m/step is applied at the top of the fillers to simulate its subsidence resulted from the groundwater decline. The physical and mechanical parameters of the materials employed in the numerical simulation are listed in Table 1.

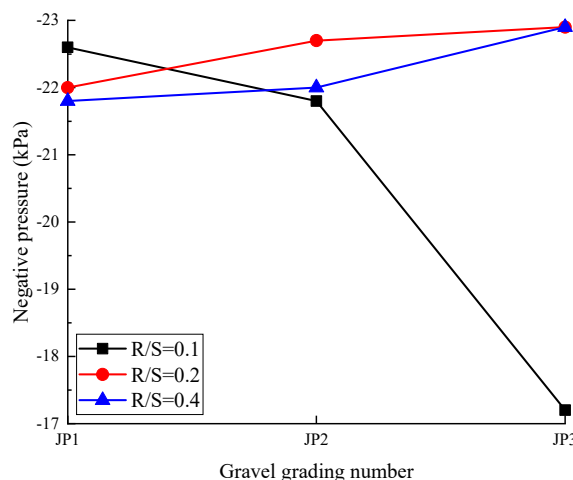


Fig. 5 Maximum negative pressure curve under different working conditions.

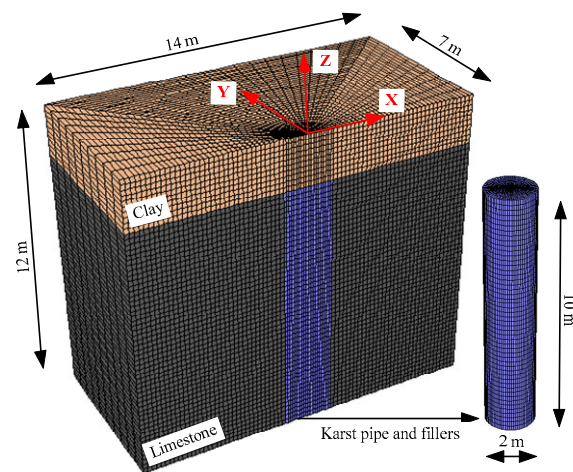


Fig. 6 Numerical model for simulating the loss of karst pipe fillers.

#### 3.2 Change law of negative pressure

The change curve of the negative pressure in the negative pressure zone with vertical displacement of the fillers is shown in Fig. 7. As the fillers settle, the

**Table 1** Physical-mechanical parameters used in the numerical simulation of the loss process of karst pipe fillers

Material	Density (g/cm <sup>3</sup> )	Bulk modulus (GPa)	Shear modulus (GPa)	Cohesion (MPa)	Tensile strength (MPa)	Internal friction angle (°)
Clay	1850	0.0017	0.0013	0.024	0.02	21
Limestone	2700	41	19	/	/	/
Fillers	1700	0.0033	0.0011	/	/	/

negative pressure in the negative pressure zone passes through three stages, namely the rapid increase stage, the rapid decrease stage and the gradual dissipation stage. Since the settlement rate of the fillers is set to be constant in the numerical simulation, no slow decrease stage of the negative pressure is observed when the groundwater decline is slowed down, as in the model tests. When the vertical settlement of the fillers reaches 4.5 cm, the negative pressure reaches the maximum of 44.86 kPa. During the rapid increase stage of negative pressure, tensile failure elements appear in the negative pressure zone. Due to the failure of this part of the soil, the negative pressure is reduced, and then the negative pressure begins to decrease rapidly. When the settlement of the fillers exceeds 8.5 cm, the pore pressure in the soil is positive, and the pore pressure fluctuates greatly for a period before it gradually becomes stable. This indicates that the negative pressure at this stage gradually decreases until it disappears.

### 3.3 Influencing factors of negative pressure

As shown in Fig. 7, under the constant simulated conditions, there is a maximum negative pressure in the negative pressure zone. Fig. 8 shows the relationship between the maximum negative pressure and the thickness of the overlying soil under the condition of a saturated and dry overlying soil layer. As the clay thickness increases, the initial pore water pressure and the gas pressure in the soil increase, thereby eliminating the created negative pressure. Therefore, the maximum negative pressure of saturated and dry clay decreases as the thickness of the overlying clay increases. Since the pore water pressure increases rapidly with depth, its offset effect on the negative pressure is more obvious. Therefore, the maximum negative pressure in saturated clay decreases more significantly as the thickness of the overlying clay increases.

The influence curve of the initial void ratio of the overlying soil on the maximum negative pressure is shown in Fig. 9. The maximum negative pressure in the soil sample initially increases and then decreases as the

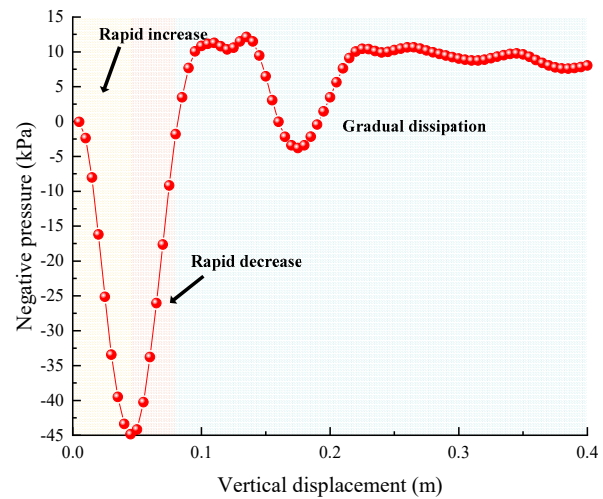


**Fig. 7** Negative pressure curve with the settlement of the fillers.

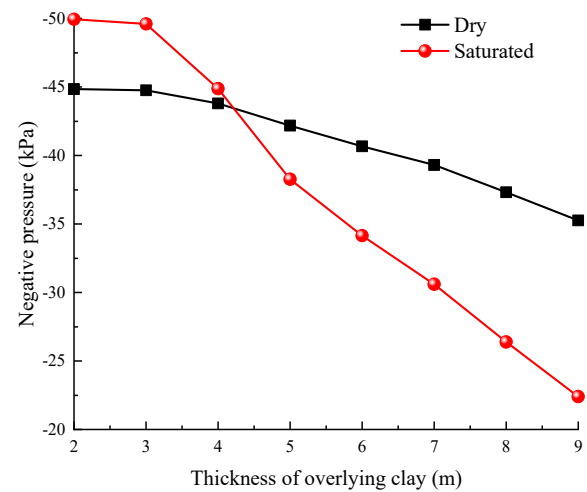


**Fig. 8** Relationship between the thickness of overlying clay and the maximum negative pressure.

initial void ratio increases. The initial void ratio of the soil sample is too small, indicating that the soil sample is relatively dense, and the movement of the soil easily leads to a large positive pore pressure in the soil, which balances the negative pressure generated, resulting in a small maximum negative pressure. The initial void ratio of the soil sample is too large, the soil sample is relatively loose, and more air is trapped in it, which reduces the negative pressure caused by the decline of the groundwater table. Therefore, an initial condition

that is too dense and too loose is not conducive to the accumulation of negative pressure in soil samples.

In addition to the thickness of the overlying soil layer and the initial void ratio, the settlement rate of the fillers also has a significant effect on the negative pressure. Fig. 10 indicates that the greater the

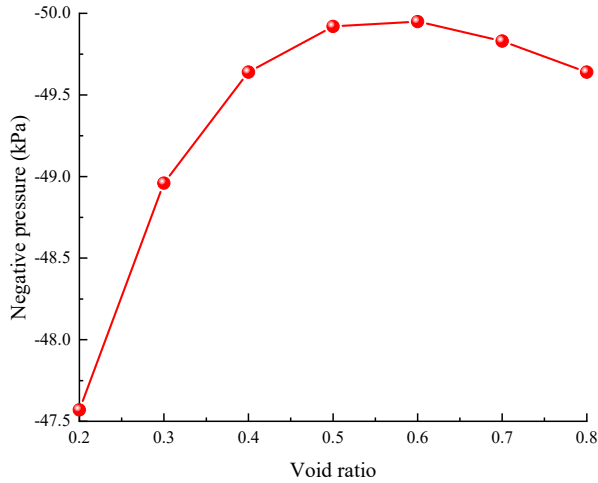


Fig. 9 Relationship between the void ratio and the maximum negative pressure.

settlement rate of the fillers, the greater the maximum negative pressure created in the overlying soil layer. In practical engineering, if the sinking rate of groundwater or fillers increases, the negative pressure in the soil increases, which has an unfavorable effect on the stability of the overlying soil layer.

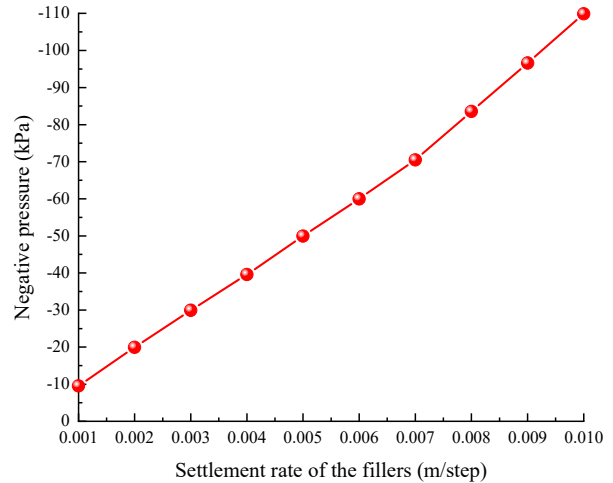


Fig. 10 Relationship between the settlement rate of the fillers and the maximum negative pressure.

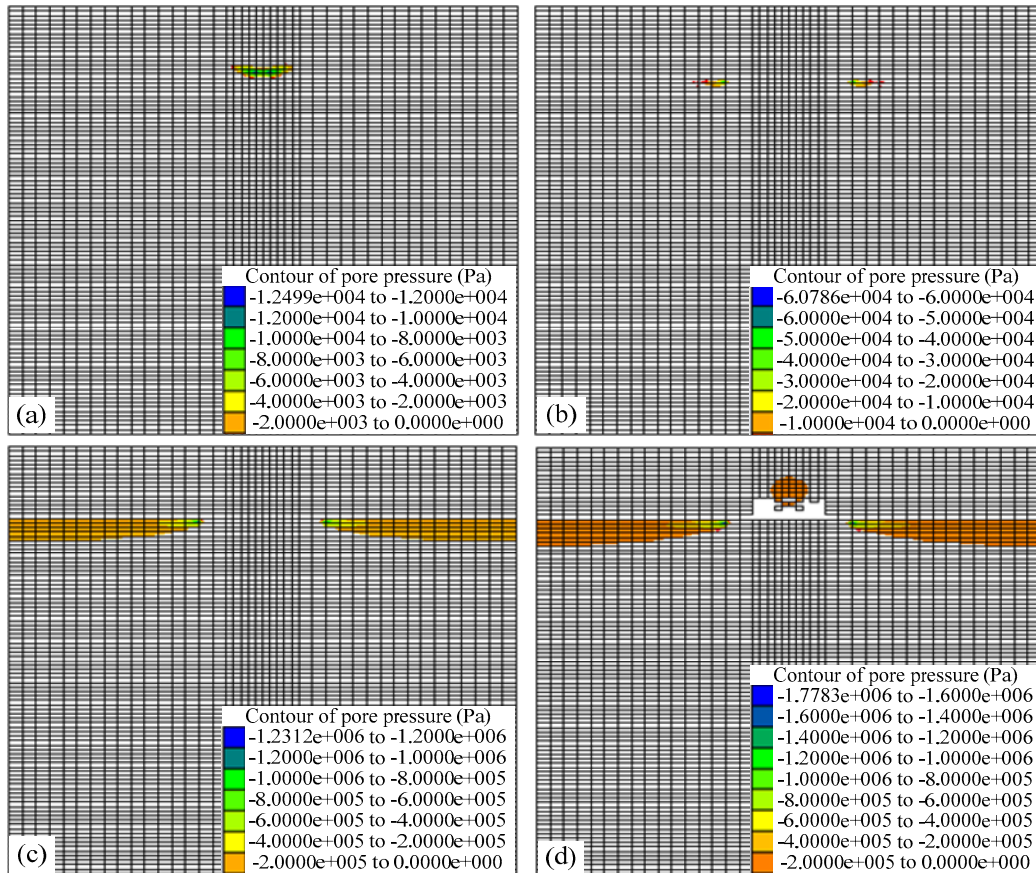


Fig. 11 Variation laws of the pore pressure during the loss process of the karst pipe fillers when the vertical displacement of the fillers is: (a) 0.004 mm, (b) 0.389 mm, (c) 6.081 mm, and (d) 31.985 mm.

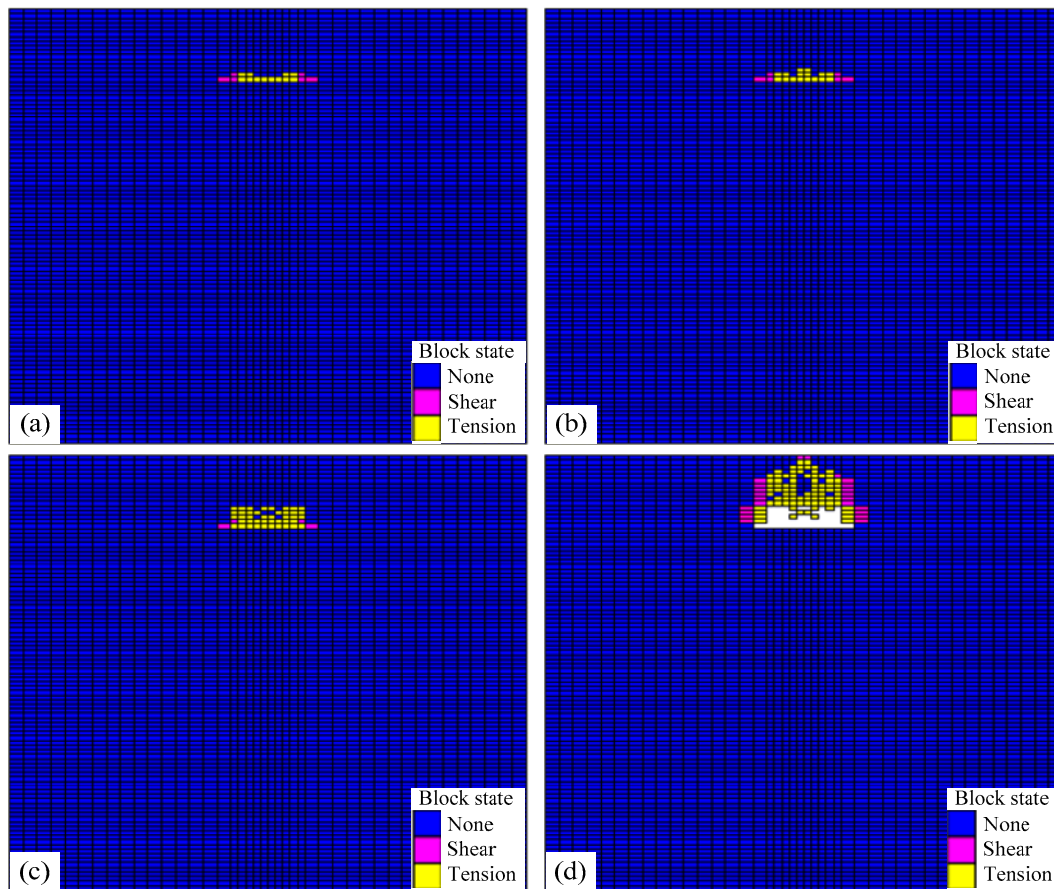
### 3.4 Formation of sinkholes

Fig. 11 and Fig. 12 show the variation laws of the pore pressure and the plastic zones, respectively. When fillers begin to sink, a negative pore pressure is created at the interface between the overlying clay and the fillers, as shown in Fig. 11a. Under the influence of negative pressure, the clay in this area shows a state of tensile failure, while shear failure elements appear on both sides of the tensile failure elements (Fig. 12a). The negative pressure in the negative pressure region gradually increases, causing the plastic zones to gradually increase, as illustrated by Fig. 12b and Fig. 12c. As the fillers settle, the negative pressure zone and surrounding soil collapse and fail, resulting in the dissipation and transfer of negative pressure. The previous negative pressure zone disappears, the new negative pressure zones arise on both sides of the fillers and the negative pressure in this area continues to increase, as shown in Fig. 11b, Fig. 11c and Fig. 11d. Since the limestone is stable and supports the overlying clay well, the increasing negative pressure in

the new negative pressure zone does not damage the clay in this area. Fig. 12d indicates that the negative pressure caused by the loss of fillers creates an arched soil hole in the clay layer. The soil hole loses its support to the layer above it, and the upper clay layer settles under its self-weight and fails.

Based on the numerical simulations and model tests, the formation mechanism of sinkholes caused by groundwater level decline in karst areas can be explained. Clearly, the decline in the groundwater level or the settlement of water-containing fillers creates a negative pressure zone underground. Under the tensile stress of negative pressure, tensile failure occurs in the soil around the negative pressure zone, creating an arched soil hole that reduces its supporting effect on the soil above. Therefore, the soil above the negative pressure zone collapses under its self-weight. Cover collapse caused by groundwater level decline in karst areas includes internal collapse and surface collapse.

The previous research shows that the negative pressure caused by the decline in the groundwater level is not infinite. Hence, the arched soil hole created by



**Fig. 12** Variation laws of the plastic zones during the loss process of the karst pipe fillers when the vertical displacement of the fillers is: (a) 0.004 mm, (b) 0.389 mm, (c) 6.081 mm, and (d) 31.985 mm.

the negative pressure lies in a certain area. The engineering geological conditions influence the negative pressure, which in turn influences the size of the arched soil hole. According to the Protodyakonov's equilibrium arch theory (PEAT), the tunnel excavation will disturb the overlying strata and form an arch-like disturbed zone in the strata. In a karst collapse, the karst pipe lies in the bedrock, and the bedrock is relatively stable. It can approximately assume that the width of the arch-like disturbed zone corresponds to the width of the karst pipe. Based on the PEAT, a simplified pressure arch model can be constructed to illustrate the mechanical conditions of the arch-like disturbed zone (Fig. 13). Point *O* is subjected to horizontal tangential force *T*, the arch foot (point *A*) bears the horizontal force *H* and the vertical force *N*. The uniform load *q*, including the overlying soil weight, the vacuum negative pressure and the vertical permeability, is distributed on the arch. The pressure arch is in equilibrium, so it can be obtained that

$$H - T = 0 \tag{1}$$

$$N - q \times R = 0 \tag{2}$$

$$T \times h_{max} - \frac{q \times R^2}{2} = 0 \tag{3}$$

where  $h_{max}$  denotes the maximum height of the pressure arch; *R* is the radius of the karst pipe. The maximum height of the pressure arch can be expressed by Eq. (4):

$$h_{max} = \frac{RN}{2H} \tag{4}$$

According to PEAT and assuming that the safety factor of against sliding is 2, Eq. (5) can be deduced:

$$2H = N \times k_f \tag{5}$$

where  $k_f$  represents the firmness coefficient of the overlying strata. The firmness coefficient  $k_f$  is an empirical index defined as the ability of a material against damage and reflects the mechanical resistance of the overlying strata in this study. By substituting Eq. (5) into Eq. (4),  $h_{max}$  can be expressed as follows:

$$h_{max} = \frac{R}{k_f} \tag{6}$$

Considering that the karst pipe is three-dimensional, Eq. (6) should be corrected to

$$h_{max} = 0.828 \frac{R}{k_f} \tag{7}$$

The firmness coefficient  $k_f$  is influenced by the mechanical properties of the overlying strata. When

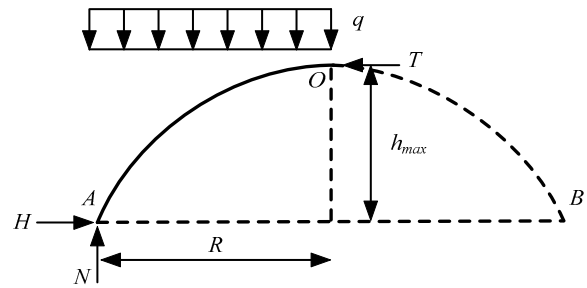


Fig. 13 Mechanical model of the pressure arch.

the overlying strata are thin and less than the maximum height of the pressure arch, internal collapse and surface collapse happen simultaneously. Otherwise, internal collapse happens first, the overlying soil collapses layer by layer, and then surface collapse happens.

#### 4 Case Study

The Yujiawan Reservoir is located in the Jingang Village, Geleshan Town, Chongqing City in China. The groundwater depth is 1.5 m below the ground surface. The predominant bedrock is limestone, and there are developed landforms such as karst caves, underground streams and ponors. There is an aquifer with an inclination of approximately 40° underground. Below the Yujiawan Reservoir, the Zhongliangshan Tunnel of the Chongqing Light Rail Line 1 enters the aquifer (Fig. 14). The reservoir was in good condition before the tunnel was excavated. According to the field tests, surface water entered the Zhongliangshan Tunnel through cracks in the limestone. On October 11, 2010, the tunnel was excavated to reach the limestone aquifer, the hydraulic discharge increased from 549.89 m<sup>3</sup>/day to 1591.64 m<sup>3</sup>/day. Between October 20, 2010 and September 13, 2015, six successive sinkholes occurred at the east of the reservoir. The six sinkholes were named P1, P2, P3, P4, P5 and P6, respectively. Actually, the formation of sinkholes is a gradual development process, which can be demonstrated by the six successive sinkholes at the Yujiawan Reservoir. Therefore, by taking the Yujiawan Reservoir as an example, this section focuses on revealing the progressive formation process and mechanism of cover collapse sinkholes related to groundwater level decline in karst areas.

The geometric parameters of collapse pits are listed in Table 2. According to the geological data of Yujiawan Reservoir, the firmness coefficient is

determined to be 3.27, and thus the theoretical height of the arched soil hole in the clay layer before the formation of sinkholes can be determined as listed in Table 2. Since the six sinkholes in the Yujiawan Reservoir are independently distributed in space, it is assumed that there is no mutual influence between each sinkhole. Therefore, the numerical models are constructed separately to study the formation process of each sinkhole. Fig. 15 is the numerical result of the arched soil hole formed in the clay layer after the filler loss. The calculated height of the arched soil hole is close to the theoretical value, and the larger theoretical value is a conservative design basis for the actual project, which is reasonable for safety reasons. Therefore, Eq. (7) can be used to estimate the height of pressure arch in practical engineering. If the thickness of the overlying strata is small, the decline in the water table can directly lead to the cover collapse. Therefore, the exploration of the thickness of overlying strata should be strengthened in karst areas.

The formation process of the six sinkholes is shown in Fig. 16. The excavation of the Zhongliangshan Tunnel resulted in a nearly threefold increase in hydraulic discharge. According to the research results shown in Fig. 10, the negative pressure generated between the clay layer and the karst pipe increased almost three times, which led to the formation of arched soil hole in the clay layer. The arched soil hole loses its support to the upper layer. The layers above collapse layer by layer under their self-weight. Tensile failures occur in the upper part of the arched soil hole, while shear failure occurs at the side of the arched soil hole. The angle between the shear failure plane and the horizontal plane is approximately  $45+\varphi/2$  (where  $\varphi$  is the internal friction angle of the clay), which is consistent with the integration of the limit equilibrium theory and the Mohr-Coulomb yield criterion.

### 5 Conclusions

In this study, the presence of negative pressure

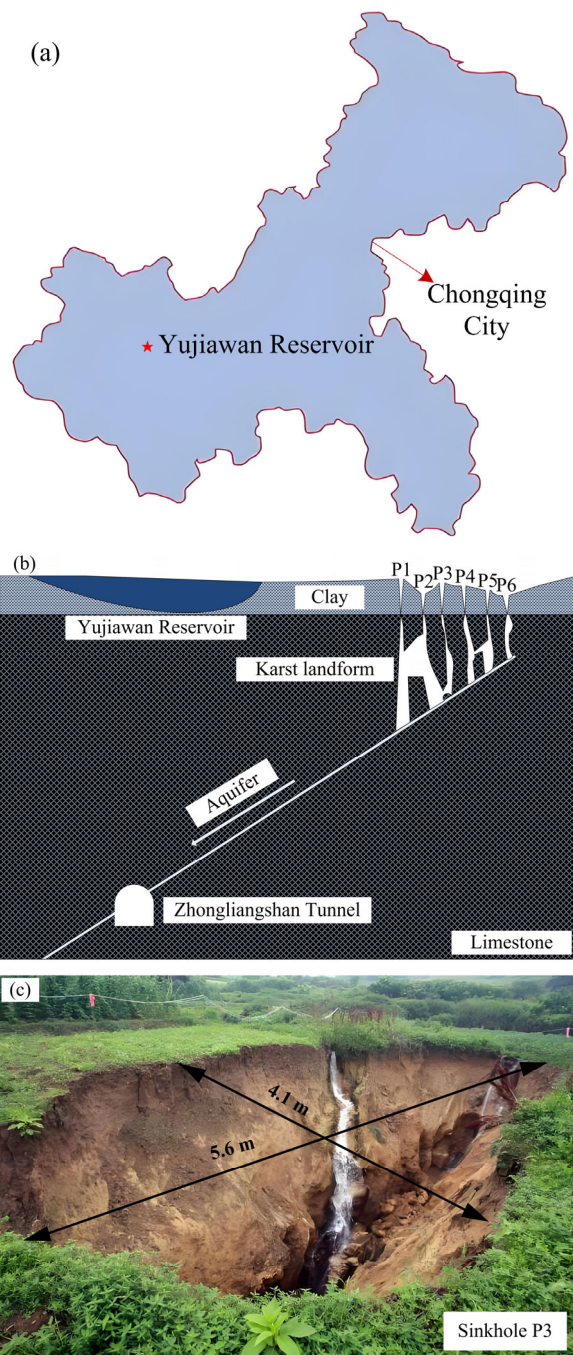


**Fig. 14** (a) Location of the Yujiawan Reservoir in the Chongqing Municipality; (b) Geological cross section of the study area; (c) On-site observation of Sinkhole P3.

**Table 2** Geometry parameters of collapse pits in the Yujiawan Reservoir

Number	Major semi axis (m)	Minor semi axis (m)	Thickness of overlying layer (m)	Theoretical height of arched soil hole (m)
P1	5.0	3.7	2.4	0.94 - 1.27
P2	3.0	1.5	1.1	0.38 - 0.76
P3	5.6	4.1	2.2	1.04 - 1.42
P4	3.2	2.1	1.8	0.53 - 0.81
P5	3.6	1.9	1.2	0.48 - 0.91
P6	2.8	1.6	0.9	0.41 - 0.71

following groundwater decline was confirmed through the designed model experiment. Subsequently, the further simulations were carried out to investigate the changing law of negative pressure as groundwater level declines and to analyze the main factors influencing

negative pressure. The conclusions can be drawn as follows:

(1) Cover collapse in karst areas is a complex environmental and geological hazard, with groundwater level decline being one of its main

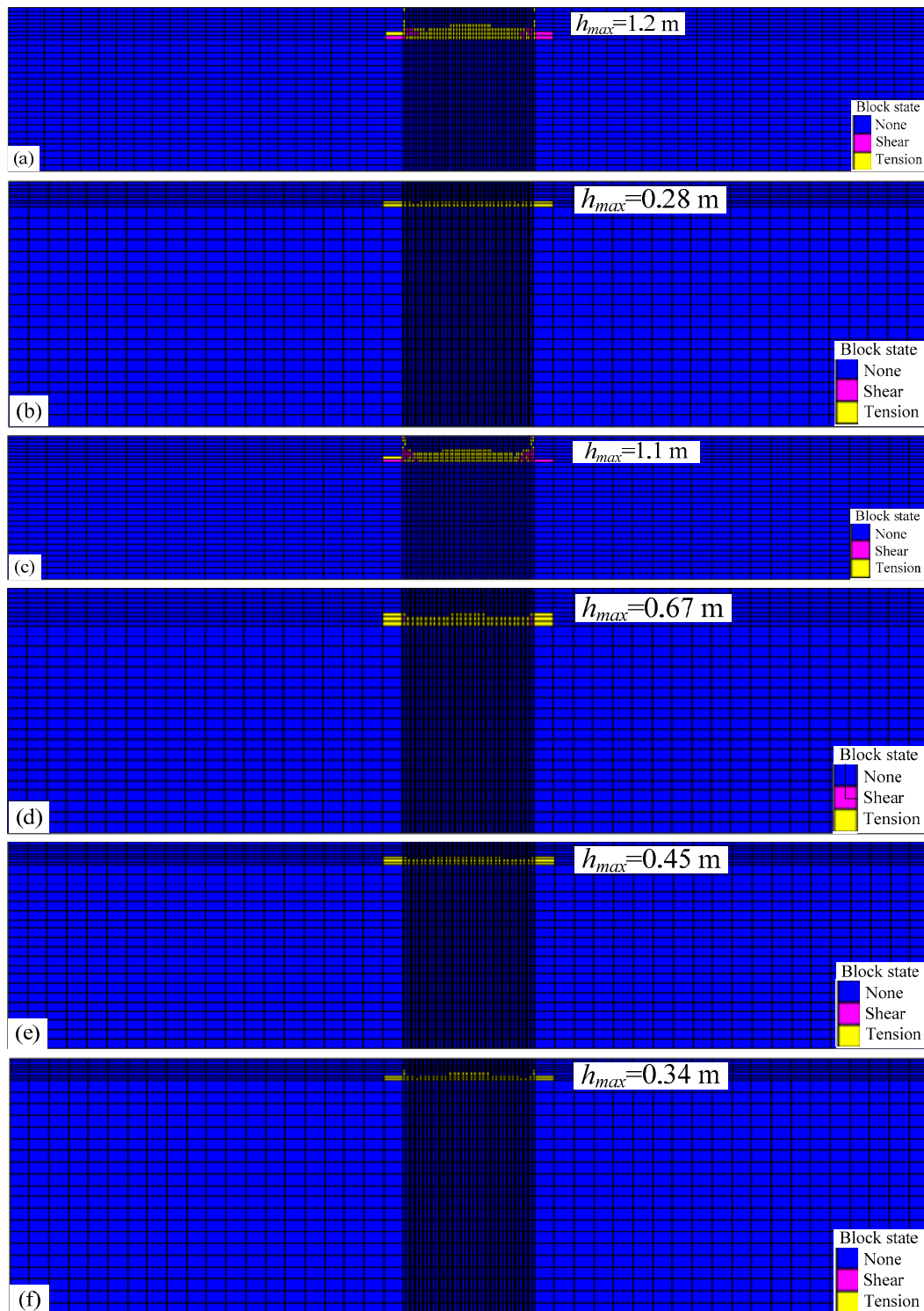


**Fig. 15** Numerical results of the arched soil holes formed in the clay layer after the decline of the groundwater level. (a) Sinkhole P1, (b) Sinkhole P2, (c) Sinkhole P3, (d) Sinkhole P4, (e) Sinkhole P5, and (f) Sinkhole P6.

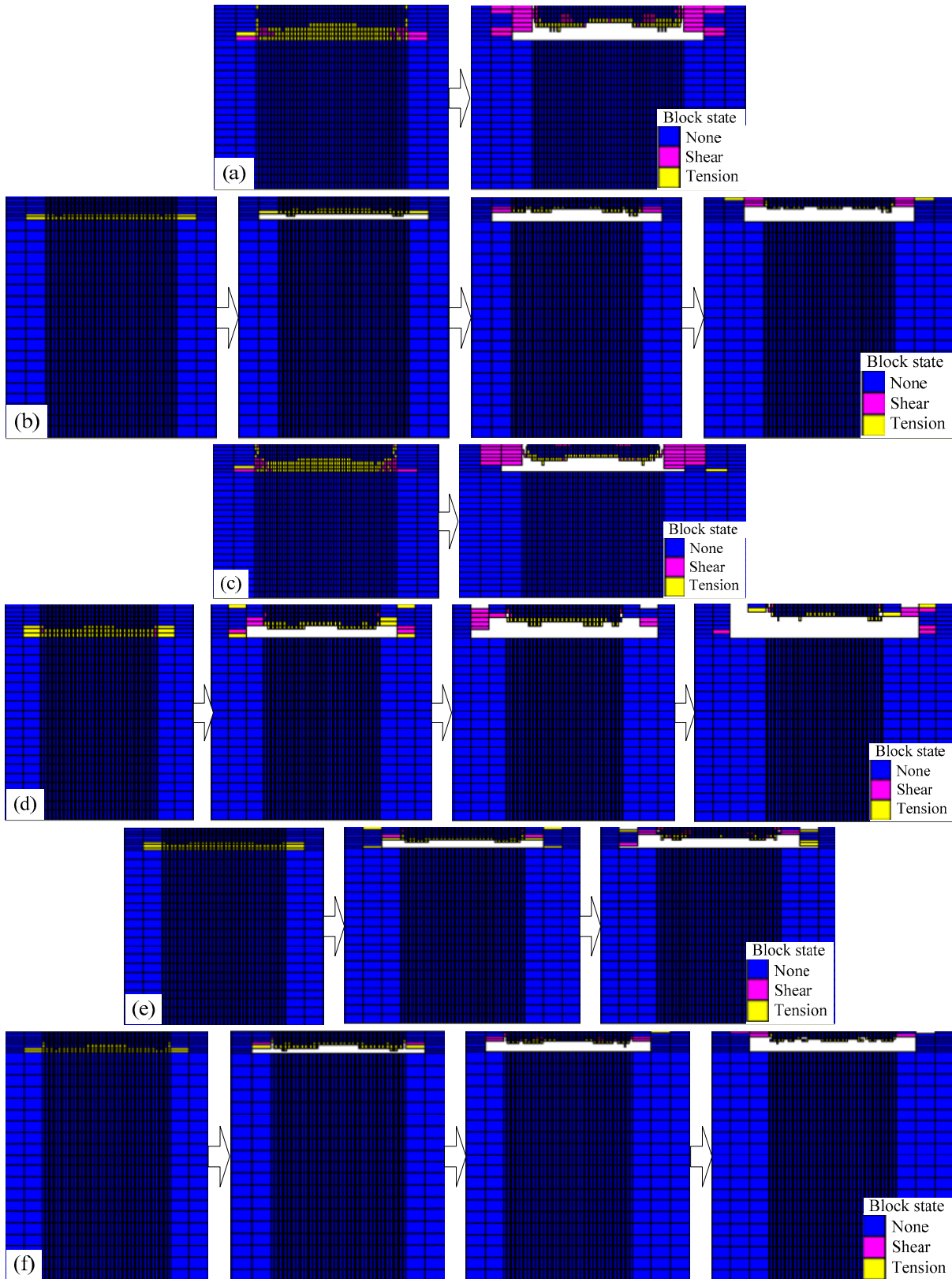


**Fig. 16** Formation process of the six sinkholes in the Yujiawan Reservoir. (a) Sinkhole P1, (b) Sinkhole P2, (c) Sinkhole P3, (d) Sinkhole P4, (e) Sinkhole P5, and (f) Sinkhole P6

triggers. The model tests have confirmed that this decline can induce negative pressure in the overlying soil. With the groundwater level dropping, the negative pressure in the overlying soil progresses through four main stages: rapid increase, slow decrease, rapid decrease, and gradual dissipation. The process reaches a maximum negative pressure, which is influenced by the void ratio of the overlying soil.

(2) The simulated results regarding the filler loss because of groundwater level decline revealed that negative pressure initially increases and then decreases. The maximum negative pressure is influenced by the rate of filler decline and the thickness and initial void ratio of the overlying strata. For both saturated and dry clay, the maximum negative pressure decreases with the thickness of the overlying layers increasing. Extremely dense or loose initial conditions of the overlying soil do not favor the accumulation of negative pressure in soil samples. An increased decline rate of fillers will lead to a rise in maximum negative pressure.

(3) The formation mechanism of cover collapse sinkholes in karst areas can be explained using the results of numerical simulations and model tests. The decline in the groundwater level or the settlement of water-containing fillers can create a negative pressure zone underground. Under the tensile stress of negative pressure, tensile failures occur in the soil around the negative pressure zone, creating an arched soil hole which will reduce its supporting effect on the soil above. Therefore, the soil above the negative pressure zone collapses under its self-weight.

(4) Cover collapse sinkholes caused by groundwater table decline in karst areas includes internal collapse and surface collapse. If the overlying strata is thin and less than the height of the pressure arch, internal collapse and surface collapse occur simultaneously. When the thickness of the overlying strata is greater than the thickness of the pressure arch, internal collapse occurs first, then the overlying soil collapses layer by layer, and finally surface collapse occurs. The geological conditions and the decline in groundwater level will influence the occurrence of internal collapse in karst areas, which should be paid more attention by engineers. The geophysical technology, borehole, drilling and groundwater level monitoring can be used by on-site engineers to detect the location and scale of karst pipelines and determine the physical and mechanical parameters of overlying soils. Limited by the geological survey technologies,

the detailed real-time monitoring data is not available for predicting the occurrence of the cover collapse sinkholes related to groundwater level decline in this study. The follow-up research can be conducted to investigate the precursor signal and early-warning strategy of cover collapse sinkholes to avoid human injuries and economic losses.

## Acknowledgments

This work was supported by the Natural Science Foundation of Shandong Province, China (Grant No. ZR2020QE110) and the National Natural Science Foundation of China, China (Grant No. 52104089).

## Author Contributions

LIU Xingzong: Formal analysis, Investigation, Writing - original draft; CHEN Hongkai: Investigation, Validation, Writing - review & editing; GONG Bin: Conceptualization, Methodology, Supervision, Writing - review & editing; JIANG Guanghui: Formal analysis, Visualization, Funding acquisition; WANG Jintao: Formal analysis, Project administration, Funding acquisition.

## Ethics Declaration

**Availability of Data/Materials:** The datasets generated and/or analyzed during the current study are available from the corresponding author upon reasonable request.

**Conflict of Interest:** The authors declare no conflict of interest.

## Open Access

This article is licensed under a Creative Commons Attribution 4.0 International License, which permits use, sharing, adaptation, distribution and reproduction in any medium or format, as long as you give appropriate credit to the original author(s) and the source, provide a link to the Creative Commons licence, and indicate if changes were made. The images or other third party material in this article are included in the article's Creative Commons licence, unless indicated otherwise in a credit line to the material. If material is not included in the article's Creative Commons licence and your intended use is not permitted by statutory

regulation or exceeds the permitted use, you will need to obtain permission directly from the copyright holder.

To view a copy of this licence, visit <http://creativecommons.org/licenses/by/4.0/>

## References

- Al-Halbouni D, Holohan EP, Taheri A, et al. (2019) Distinct element geomechanical modelling of the formation of sinkhole clusters within large-scale karstic depressions. *Solid Earth* 10(4): 1219-1241.  
<https://doi.org/10.5194/se-10-1219-2019>
- Brahmi S, Fehdi C, Hadji R, et al. (2023) Hamad karst-induced sinkhole detection using a tomography imaging survey, case of Setifian High Plain, NE Algeria. *Geotech Geol Eng* 41: 1961-1976.  
<https://doi.org/10.1007/s10706-023-02384-x>
- Chen B, Gong B, Wang S, et al. (2022) Research on zonal disintegration characteristics and failure mechanisms of deep tunnel in jointed rock mass with strength reduction method. *Mathematics* 10: 922.  
<https://doi.org/10.3390/math10060922>
- Dai JL, Lei MT (2018) Standard guide for karst collapse investigation and its technical essential. *Environ Earth Sci* 77(4): 133.  
<https://doi.org/10.1007/s12665-018-7288-7>
- di Santolo AS, Forte G, Santo A (2018) Analysis of sinkhole triggering mechanisms in the hinterland of Naples (Southern Italy). *Eng Geol* 237: 42-52.  
<https://doi.org/10.1016/j.enggeo.2018.02.014>
- Dong SN, Wang H, Zhou WF (2020) Sinkholes and their impacts on karst hydrogeology in a peatland complex of Northern Ontario, Canada. *Carbonates Evaporites* 35: 50.  
<https://doi.org/10.1007/s13146-020-00582-9>
- Feng X, Gong B, Liang Z, et al. (2024) Study of the dynamic failure characteristics of anisotropic shales under impact Brazilian splitting. *Rock Mech Rock Eng* 57: 2213-2230.  
<https://doi.org/10.1007/s00603-023-03673-w>
- Festa V, Fiore A, Parise M, et al. (2012) Sinkhole evolution in the Apulian Karst of Southern Italy: a case study, with some considerations on Sinkhole Hazards. *J Cave Karst Stud* 74(2): 137-147.  
<https://doi.org/10.4311/2011JCKS0211>
- Galve JP, Remondo J, Gutierrez F (2011) Improving sinkhole hazard models incorporating magnitude-frequency relationships and nearest neighbor analysis. *Geomorphology* 134(1-2): 157-170.  
<https://doi.org/10.1016/j.geomorph.2011.05.020>
- Gao M, Gong B, Liang Z, et al. (2023) Investigation of the anisotropic mechanical response of layered shales. *Energy Sci Eng* 11(12): 4737-4754.  
<https://doi.org/10.1002/ese3.1611>
- Gong B, Liang Z, Liu X (2022) Nonlinear deformation and failure characteristics of horseshoe-shaped tunnel under varying principal stress direction. *Arab J Geosci* 15: 475.  
<https://doi.org/10.1007/s12517-022-09678-z>
- Gong B, Zhao T, Thusyanthan I, et al. (2024) Modelling rock fracturing by a novel implicit continuous to discontinuous method. *Comput Geotech* 166: 106035.  
<https://doi.org/10.1016/j.compgeo.2023.106035>
- Guo S, Jiang YH, Tang X, et al. (2023) Experimental study on the soil erosion through a defective pipe under the cyclic infiltration-exfiltration flow. *Transp Geotech* 42: 101085.  
<https://doi.org/10.1016/j.trgeo.2023.101085>
- Guo S, Shao Y, Zhang TQ, et al. (2014) Physical modeling on sand erosion around defective sewer pipes under the influence of groundwater. *J Hydraul Eng* 139(12): 1247-1257.  
[https://doi.org/10.1061/\(ASCE\)HY.1943-7900.0000785](https://doi.org/10.1061/(ASCE)HY.1943-7900.0000785)
- Gutierrez F, Guerrero J, Lucha P (2008) Quantitative sinkhole hazard assessment. A case study from the Ebro Valley evaporite alluvial karst (NE Spain). *Nat Hazards* 45: 211-233.  
<https://doi.org/10.1007/s11069-007-9161-y>
- Gutierrez F, Parise M, Waele DJ, et al. (2014) A review on natural and human-induced geohazards and impacts in karst. *Earth-Sci Rev* 138: 61-88.  
<https://doi.org/10.1016/j.earscirev.2014.08.002>
- He KQ, Jia YY, Wang B, et al. (2013) Comprehensive fuzzy evaluation model and evaluation of the karst collapse susceptibility in Zaozhuang Region, China. *Nat Hazards* 68(2): 613-629.  
<https://doi.org/10.1007/s11069-013-0653-7>
- He KQ, Jia YY, Zhao M, et al. (2012) Comprehensive analysis and quantitative evaluation of the influencing factors of karst collapse in groundwater exploitation area of Shiliquan of Zaozhuang, China. *Environ Earth Sci* 66(8): 2531-2541.  
<https://doi.org/10.1007/s12665-012-1675-2>
- He KQ, Liu CL, Wang SJ (2002) Karst collapse related to over-pumping and a criterion for its stability. *Environ Geol* 43: 720-724.  
<https://doi.org/10.1007/s00254-002-0669-x>
- He KQ, Zhang SQ, Wang F, et al. (2010) The karst collapses induced by environmental changes of the groundwater and their distribution rules in North China. *Environ Earth Sci* 61(5): 1075-1084.  
<https://doi.org/10.1007/s12665-009-0429-2>
- Howari FM, Aldouri R, Sadiq A (2016) Gravity investigations of recent sinkholes and karst pits of Dahal Al-Hamam, State of Qatar. *Environ Earth Sci* 75(5): 440.  
<https://doi.org/10.1007/s12665-016-5298-x>
- Jia L, Li LJ, Meng Y, et al. (2018) Responses of cover-collapse sinkholes to groundwater changes: a case study of early warning of soil cave and sinkhole activity on Datansha Island in Guangzhou, China. *Environ Earth Sci* 77(13): 488.  
<https://doi.org/10.1007/s12665-018-7603-3>
- Jia L, Meng Y, Li LJ, et al. (2021) A multidisciplinary approach in cover-collapse sinkhole analyses in the mantle karst from Guangzhou City (SE China). *Nat Hazards* 108(1): 1389-1410.  
<https://doi.org/10.1007/s11069-021-04738-1>
- Jiang XZ, Lei MT, Gao YL (2017) Formation mechanism of large sinkhole collapses in Laibin, Guangxi, China. *Environ Earth Sci* 76(24): 823.  
<https://doi.org/10.1007/s12665-017-7128-1>
- Jiang XZ, Lei MT, Gao YL (2018) New karst sinkhole formation mechanism discovered in a mine dewatering area in Hunan, China. *Mine Water Environ* 37(3): 625-635.  
<https://doi.org/10.1007/s10230-017-0486-9>
- Jiang XZ, Lei MT, Zhao HQ (2019) Review of the advanced monitoring technology of groundwater-air pressure (enclosed potentiometric) for karst collapse studies. *Environ Earth Sci* 78(24): 701.  
<https://doi.org/10.1007/s12665-019-8716-z>
- Kharisova O, Kharisov T (2021) Searching for possible precursors of mining-induced ground collapse using long-term geodetic monitoring data. *Eng Geol* 289: 106173.  
<https://doi.org/10.1016/j.enggeo.2021.106173>
- Lago AL, Borges WR, Barros JS, et al. (2022) GPR application for the characterization of sinkholes in Teresina, Brazil. *Environ Earth Sci* 81(4): 132.  
<https://doi.org/10.1007/s12665-022-10265-4>
- Liang Y, Chen XY, Yang JS, et al. (2020) Analysis of ground collapse caused by shield tunnelling and the evaluation of the reinforcement effect on a sand stratum. *Eng Fail Anal* 115: 104616.  
<https://doi.org/10.1016/j.engfailanal.2020.104616>
- Liu R, Sun HF, Qin JW, et al. (2023) A multi-geophysical

- approach to assess potential sinkholes in an urban area. *Eng Geol* 318: 107100.  
<https://doi.org/10.1016/j.enggeo.2023.107100>
- Liu X, Gong B, Song K, et al. (2024) Indirect tensile strength test on heterogeneous rock using square plate sample with a circular hole. *Lithosphere* 2024(3).  
[https://doi.org/10.2113/2024/lithosphere\\_2023\\_322](https://doi.org/10.2113/2024/lithosphere_2023_322)
- Luu LH, Noury G, Benseghier Z, et al. (2019) Hydro-mechanical modeling of sinkhole occurrence processes in covered karst terrains during a flood. *Eng Geol* 260: 105249.  
<https://doi.org/10.1016/j.enggeo.2019.105249>
- Malinowska AA, Witkowski WT, Hejmanowski R, et al. (2019) Sinkhole occurrence monitoring over shallow abandoned coal mines with satellite-based persistent scatterer interferometry. *Eng Geol* 262:105336.  
<https://doi.org/10.1016/j.enggeo.2019.105336>
- Margiotta S, Negri S, Parise M, et al. (2016) Karst geosites at risk of collapse: the sinkholes at Nociglia (Apulia, SE Italy). *Environ Earth Sci* 75(1): 8.  
<https://doi.org/10.1007/s12665-015-4848-y>
- Maroof MA, Mahboubi A, Vincens E, et al. (2022) Effects of particle morphology on the minimum and maximum void ratios of granular materials. *Granular Matter* 24: 41.  
<https://doi.org/10.1007/s10035-021-01189-0>
- Meng Y, Li ZJ, Jia L (2020) An analysis of allowable groundwater drawdown and pumpage from a karst aquifer to prevent sinkhole collapses in the Pearl River Delta, China. *Water Resour* 47(4): 530-536.  
<https://doi.org/10.1134/S0097807820040089>
- Pan ZY, Chen XJ, Yang X, et al. (2022) Formation mechanism analysis of cover collapse sinkholes in Wugaishan Town, Chenzhou City, Hunan province, China. *Environ Earth Sci* 81(2): 48.  
<https://doi.org/10.1007/s12665-022-10171-9>
- Pan ZY, Jiang XZ, Lei MT, et al. (2018) Mechanism of sinkhole formation during groundwater-level recovery in karst mining area, Dachengqiao, Hunan province, China. *Environ Earth Sci* 77(24): 799.  
<https://doi.org/10.1007/s12665-018-7987-0>
- Pai L, Wu H, Wang X (2023) Shaking table test and cumulative deformation evaluation analysis of a tunnel across the hauling sliding surface. *Deep Undergr Sci Eng* 2(4): 371-393.  
<https://doi.org/10.1002/dug2.12046>
- Peng SG, Huang WR, Luo GY, et al. (2023) Failure mechanisms of ground collapse caused by shield tunnelling in water-rich composite sandy stratum: A case study. *Eng Fail Anal* 146: 107100.  
<https://doi.org/10.1016/j.engfailanal.2023.107100>
- Qin YW, Shang CK, Li X, et al. (2023) Failure mechanism and countermeasures of rainfall-induced collapsed shallow loess tunnels under bad terrain: A case study. *Eng Fail Anal* 152: 107477.  
<https://doi.org/10.1016/j.engfailanal.2023.107477>
- Seol H, Won D, Jang J, et al. (2022) Ground collapse in EPB shield TBM site: A case study of railway tunnels in the deltaic region near Nak-Dong River in Korea. *Tunn Undergr Sp Tech* 120: 104274.  
<https://doi.org/10.1016/j.tust.2021.104274>
- Talib OC, Shimon W, Sarah K, et al. (2022) Detection of sinkhole activity in West-Central Florida using InSAR time series observations. *Remote Sens Environ* 269: 112793.  
<https://doi.org/10.1016/j.rse.2021.112793>
- Wang YY, Gong B, Tang CA, et al. (2023) Size effect and lateral pressure effect on the mechanical resistance of columnar jointed basalt. *Int J Rock Mech Min Sci* 171: 105571.  
<https://doi.org/10.1016/j.ijrmms.2023.105571>
- Wang X, Zhang Y, Feng C, et al. (2024) Continuous-discontinuous analysis of bench blasting in open-pit mining: Influences of hole packing and caving holes. *Rock Mech Bull* 3(4): 100142.  
<https://doi.org/10.1016/j.rockmb.2024.100142>
- Wei YY, Sun SL (2018) Comprehensive critical mechanical model of covered karst collapse under the effects of positive and negative pressure. *B Eng Geol Environ* 77(1): 177-190.  
<https://doi.org/10.1007/s10064-016-0995-y>
- White WB (2002) Karst hydrology: recent developments and open questions. *Eng Geol* 65: 85-105.  
[https://doi.org/10.1016/S0013-7952\(01\)00116-8](https://doi.org/10.1016/S0013-7952(01)00116-8)
- Xia KZ, Chen CX, Zheng Y, et al. (2019) Engineering geology and ground collapse mechanism in the Chengchao Ironore Mine in China. *Eng Geol* 249: 129-147.  
<https://doi.org/10.1016/j.enggeo.2018.12.028>
- Xiao XX, Xu M, Ding QZ, et al. (2018) Experimental study investigating deformation behavior in land overlying a karst cave caused by groundwater level changes. *Environ Earth Sci* 77(3): 64.  
<https://doi.org/10.1007/s12665-017-7102-y>
- Xu C, Wang S, Xia C (2024) Analytical prediction for time-dependent interaction of a circular tunnel excavated in strain-softening rock mass. *Rock Mech Bull* 3(3): 100127.  
<https://doi.org/10.1016/j.rockmb.2024.100127>
- Yacine A, Med Ridha M, Laid HM, et al. (2014) Karst Sinkholes Stability Assessment in Cheria Area, NE Algeria. *Geotech Geol Eng* 32: 363-374.  
<https://doi.org/10.1007/s10706-013-9719-2>
- Yao W, Wang E, Liu X, et al. (2022) Fracture distribution in overburden strata induced by underground mining. *Deep Undergr Sci Eng* 1(1): 58-64.  
<https://doi.org/10.1002/dug2.12021>
- Yu J, Gong B, Cao C, et al. (2024) A novel cohesive interlayer model considering friction. *Int J Solids Struct* 113049.  
<https://doi.org/10.1016/j.ijsolstr.2024.113049>
- Yu C, Gong B, Wu N, et al. (2022) Simulation of the Fracturing Process of Inclusions Embedded in Rock Matrix under Compression. *Appl Sci* 12, 8041.  
<https://doi.org/10.3390/app12168041>
- Zeng YF, Zhou WF (2019) Sinkhole remedial alternative analysis on karst lands. *Carbonate Evaporite* 34(1): 159-173.  
<https://doi.org/10.1007/s13146-018-0467-5>
- Zhang C, Chen Y, Wang Y, et al. (2024) Discrete element method simulation of granular materials considering particle breakage in geotechnical and mining engineering: A short review. *Green Smart Min Eng* 1(2): 190-207.  
<https://doi.org/10.1016/j.gsme.2024.06.003>
- Zhang JS, Xu MY, Cui MH, et al. (2022) Prediction of ground subsidence caused by shield tunnel construction under hidden karst cave. *Geotech Geol Eng* 40: 3839-3850.  
<https://doi.org/10.1007/s10706-022-02136-3>
- Zhang Y, Zhang W, Xia H, et al. (2023) Case study and risk assessment of water inrush disaster in Qingdao metro line 4. *Appl Sci* 13: 3384.  
<https://doi.org/10.3390/app13063384>
- Zhao HJ, Ma FS, Guo J (2012) Regularity and formation mechanism of large-scale abrupt karst collapse in southern China in the first half of 2010. *Nat Hazards* 60(3): 1037-1054.  
<https://doi.org/10.1007/s11069-011-9888-3>
- Zhou WF, Beck BF (2005) Roadway construction in karst areas: management of stormwater runoff and sinkhole risk assessment. *Environ Geol* 47: 1138-1149.  
<https://doi.org/10.1007/s00254-005-1252-z>
- Zhu HZ (2024) Ground fissure development regularity and formation mechanism of shallow buried coal seam mining with Karst landform in Jiaozui coal mine: a case study. *J Mt Sci* 20(10): 3101-3120.  
<https://doi.org/10.1007/s11629-023-8197-0>
- Zumpano V, Pisano L, Parise M (2019) An integrated framework to identify and analyze karst sinkholes. *Geomorphology* 332: 213-225.  
<https://doi.org/10.1016/j.geomorph.2019.02.013>